



**HAL**  
open science

## **Asthenospheric imprints on the lithosphere in Central Mongolia and Southern Siberia from a joint inversion of gravity and seismology (MOBAL experiment)**

C. Tiberi, Anne Deschamps, Jacques Déverchère, C. Petit, Julie Perrot, D. Appriou, V. Mordvinova, T. Dugaarma, M. Ulzibaat, A. A. Artemiev

### ► **To cite this version:**

C. Tiberi, Anne Deschamps, Jacques Déverchère, C. Petit, Julie Perrot, et al.. Asthenospheric imprints on the lithosphere in Central Mongolia and Southern Siberia from a joint inversion of gravity and seismology (MOBAL experiment). *Geophysical Journal International*, 2008, 175 (3), pp.1283-1297. 10.1111/j.1365-246X.2008.03947.x . insu-00354683

**HAL Id: insu-00354683**

**<https://insu.hal.science/insu-00354683>**

Submitted on 7 Mar 2021

**HAL** is a multi-disciplinary open access archive for the deposit and dissemination of scientific research documents, whether they are published or not. The documents may come from teaching and research institutions in France or abroad, or from public or private research centers.

L'archive ouverte pluridisciplinaire **HAL**, est destinée au dépôt et à la diffusion de documents scientifiques de niveau recherche, publiés ou non, émanant des établissements d'enseignement et de recherche français ou étrangers, des laboratoires publics ou privés.

# Asthenospheric imprints on the lithosphere in Central Mongolia and Southern Siberia from a joint inversion of gravity and seismology (MOBAL experiment)

C. Tiberi,<sup>1,2</sup> A. Deschamps,<sup>3</sup> J. Déverchère,<sup>4,5</sup> C. Petit,<sup>2</sup> J. Perrot,<sup>4,5</sup> D. Appriou,<sup>4,5</sup> V. Mordvinova,<sup>6</sup> T. Dugaarma,<sup>7</sup> M. Ulzibaat<sup>7</sup> and A. A. Artemiev<sup>6</sup>

<sup>1</sup>CNRS, UMR 7072, Laboratoire de Tectonique, F-75005, Paris, France

<sup>2</sup>UPMC Université Paris 06, UMR 7072, Laboratoire de Tectonique, F-75005, Paris, France. E-mail: christal.tiberi@lgs.jussieu.fr

<sup>3</sup>Géosciences Azur, UMR CNRS 6526, UNS, CNRS, IRD, UPMC, OCA, F-06560 Sophia Antipolis, France

<sup>4</sup>Université Européenne de Bretagne, France

<sup>5</sup>Université Brest; CNRS, UMR 6538 Domaines Océaniques, Institut Universitaire Européen de la Mer, Place Copernice, 292 80 Plouzané, France

<sup>6</sup>Institute of the Earth's Crust, Siberian Branch of Russian Academy of Sciences, Irkutsk, Russia

<sup>7</sup>Research Centre of Astronomy and Geophysics, Mongolian Academy of Science, Ulaanbaatar, Mongolia

Accepted 2008 August 15. Received 2008 July 8; in original form 2008 March 13

## SUMMARY

We present a joint inversion of gravity and teleseismic data to enlighten the lithospheric structures of the Baikal–Mongolia region, an area characterized by high topographic contrasts, sporadic Cenozoic volcanism, extension and large transcurrent faulting in the vicinity of the Baikal Rift, Central Asia. The study uses a 1000 km long seismic transect that cross-cuts the main tectonic structures from north to south (namely, the Siberian platform, Tunka basin, Hangay Dome and Gobi–Altai belt).

The Siberian platform depicts a high-velocity lithosphere down to about 150 km. We evidence strong velocity contrasts within the crust below the Hangay Dome and the Tunka depression, interpreted as a thickened crust. A low-velocity/density region is located at various depths below the Hangay Dome. Thanks to the dense spatial coverage of gravity data, we are able to define the 3-D geometry of this particular low-velocity/density anomaly. The Hangay Dome anomalous body extends from 60 to 225 km depth at his largest point and slightly thins to no more than 40 km at its easternmost end. A deep low-velocity zone (below 150 km) with only a weak negative density contrast is observed on the eastern part of the transect.

We propose that the late Cenozoic uplift of the whole Mongolian Plateau and associated rifting, magmatism, high heat flow and lithospheric thinning are not externally driven by the India–Asia collision, but results from the interaction of two mantle plumes with the overlying lithosphere. Conversely, recent faulting may be the major expression of the India–Asia collision in this region, as well as N–S striking rift basins that connect and interact with major strike-slip faults, such as the Bolnai fault.

The comparison between time residuals of this experiment and the Baikal Rift seismic data shows an undeniable disproportion for the Hangay anomaly. The Hangay time residuals are far more positive than through the Baikal, arguing for an asthenospheric signature that is not seen beneath the Baikal Rift. Furthermore, the southern edge of the thick Siberian cratonic lithosphere may favour the rise of a sublithospheric mantle flow at the contact with the Baikal–Mongolia lithosphere.

**Key words:** Gravity anomalies and Earth structure; Seismic tomography; Continental tectonics: extensional; Dynamics of lithosphere and mantle; Dynamics: gravity and tectonics; Asia.

## 1 INTRODUCTION

The origin of intracontinental deformation remains a key question for tectonics and is still subject to much debate within the commu-

nity. Particularly for continental regions undergoing compressive stresses, the causes of the observed topography have been investigated through many different methods and have led to strikingly contrasted models. Among others, some involve rigid motions of

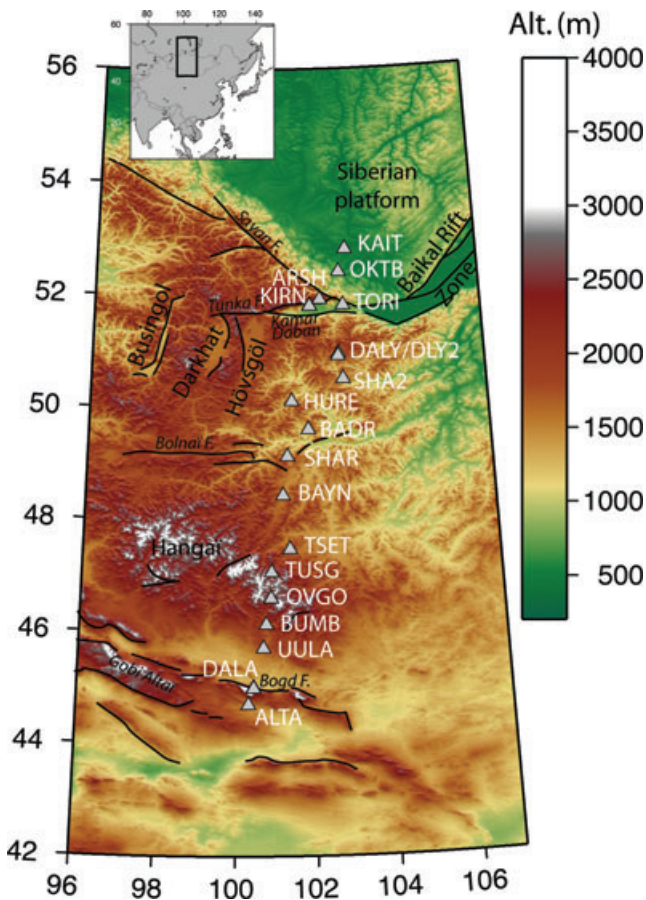


**Figure 1.** Topography and main tectonic structures in the Baikal–Mongolia region. The triangles represent the broad-band seismic stations installed in 2003 for the MOBAL experiment. Their names are indicated in white. Main tectonic and geological features are noted in black letters. Main faults are located with their names on it. Topography is taken from GTOPO30.

lithospheric blocks along narrow fault zones (e.g. Peltzer & Saucier 1996), shortening by folding, simple or pure shear, often associated with flexure (e.g. Burov *et al.* 1993; Cloetingh *et al.* 1999; Caporali 2000), continuously deforming solids (e.g. England & Molnar 1997; Flesch *et al.* 2000) and lithospheric or asthenospheric buoyancy support (e.g. Molnar *et al.* 1993; Marotta *et al.* 1998; Yin 2000).

Central Asia is clearly a key place to study intracontinental deformation because it exhibits high and young topography associated with major active tectonic features (Fig. 1). The Altai and Gobi-Altai mountains are long and narrow belts with numerous active thrust and strike-slip faults accommodating part (~1/5) of the India–Eurasia convergence (Calais *et al.* 2003) since less than 8 Ma (Vassallo *et al.* 2007); they are therefore one of the youngest mountain belts in Central Asia. The so-called Mongolian Plateau (Windley & Allen 1993) dominates much of western Mongolia (average elevation 2000 m) and depicts elevated bulges with dome shapes that are not clearly linked to any recent fault activity (Cunningham 2001; Petit *et al.* 2002). The most prominent one is the Hangay Dome (Fig. 1), an 800 × 550 km wide topographic bulge, exceeding the regional average altitude by ~1.5 km and culminating at ~4000 m. The presence of sparse Cenozoic and Quaternary volcanism (Kiselev 1987), relatively high heat flow (Khutorsky

& Yarmoluk 1989) and low-velocity zones under the crust (Yanovskaya & Kozhevnikov 2003) have led some authors to infer the existence of asthenospheric diapirs or an isolated mantle plume interacting with the lithosphere (Logatchev & Zorin 1987; Windley & Allen 1993; Cunningham 1998). Some authors have proposed that this active diapir may extend northwards beneath the southernmost Baikal Rift Zone and along the major suture zone between the Siberian Craton and the Sayan–Baikal mobile belt (e.g. Logatchev & Zorin 1987; Villaseñor *et al.* 2001) or even beneath the Craton (Zhao *et al.* 2006).

However, little is known about the detailed lithospheric and asthenospheric structure beneath Mongolia, which leaves many uncertainties on the origin of this major intracontinental relief and on its relationships with the Cenozoic rifting. In 2003, a collaborative work, including Russian, Mongolian and French institutions, aimed to prospect and image this structure along a major seismic transect that crosses Central Mongolia in a north–south (N–S) direction. The purpose of this project called Mongolian–Baikal Lithospheric (MOBAL) seismic experiment (Fig. 1) was to determine the detailed lithospheric structure beneath Mongolia and the Siberian Craton from different geophysical methods. This study presents the outcomes from this collaboration. We performed a joint inversion of gravity and seismological data along the MOBAL transect to image velocity and density anomalies within the lithosphere, leading to discussion on the origin of the topography. Using the two complementary data sets, we search for potential zones of light and hot mantle material opposite to the dense and cold cratonic lithosphere expected beneath the Siberian platform. We then discuss our results in terms of mantle heterogeneities, taking into account the resolution of our method.

## 2 TECTONIC AND GEOLOGICAL SETTINGS

### 2.1 Topography, geology and tectonics

Mongolia covers a large area, where active tectonics is marked by the progressive transition from south to north, from thrusting to strike-slip faulting and finally to extension against the eastern border of the Siberian Craton (Delouis *et al.* 2002, Fig. 1). Indeed, northeast of this region, the Baikal Rift Zone develops along the major suture zone, delimiting the Palaeo-Mesozoic Sayan–Baikal folded system and the Archean Siberian Craton (Fig. 1, Logatchev & Zorin 1992). The Baikal Rift started to develop during the Oligocene, with an increasing extension rate since the late Miocene (Petit & Déverchère 2006 and references therein). Its western end consists of a series of rifts whose orientations rotate from east–west (E–W) to almost N–S: the Tunka basin, Hövsögöl, Darkhat and Busingol rifts (Fig. 1).

The Altai and Gobi-Altai mountains delimit the southern edge of Mongolia by a well-defined 2500-m-high, 1500-km-long WNW–ESE trending range. This belt develops on various accreted Palaeozoic terranes (e.g. Zonenshain *et al.* 1990; Zorin 1999) and hosts most of the recent tectonics of this region with numerous active wrench and reverse faults, which have been active since ~8 Ma (e.g. Bayasgalan *et al.* 1999; Vassallo *et al.* 2007). North and east of these mountains, the Hangay Dome is a 500-km-long topographic high with a relatively flat plateau culminating at ~4000 m (Fig. 1). The basement of the Hangay Dome is an old Precambrian continental block, overlain by thick Palaeozoic turbidites and intensely intruded by Permian granitoids (e.g. Zorin 1999; Cunningham 2001). The most recent formations are of Cenozoic age and consist mainly of

basaltic emissions and shallow basin sediments. Low tectonic activity is observed in the Hangay Dome, and only a few normal faults bound its southern flank (Cunningham 2001).

## 2.2 Volcanism and thermal structure

Since Miocene times, Asia has been affected by volcanism. In particular, Cenozoic and Quaternary volcanism is diffuse in Mongolia, and volcanic patches are mainly concentrated in Sayan and Hövsgöl regions and around the Hangay Dome (Kiselev 1987). No time dependence is observed in the composition of the lavas, and their geochemistry suggests a deep metasomatized lithospheric origin with a possible asthenospheric component (Schlupp 1996; Ionov 2002; Barry *et al.* 2003).

Heat flow was measured in some places (Khutorskoy & Yamoluk 1989) and allows one to distinguish three different provinces: the Hövsgöl province shows high heat flow values reaching more than  $90 \text{ mW m}^{-2}$  in some places; the Baikal Rift Zone depicts moderate to high values, but lower than those from the Hövsgöl region, and Central Mongolia (Hangay Dome) exhibits heat flow values ranging between 40 and  $70 \text{ mW m}^{-2}$ , with a minimum located in the Altai and Gobi-Altai mountains.

Information on the thermal state of Mongolia has been retrieved by studies on the xenoliths. Volcanism in Mongolia brought numerous xenoliths to the surface.  $P$ - $T$  equilibrium conditions of lower crust xenoliths suggest an average crustal thickness of 46 km over western Mongolia, reaching  $\sim 50$  km north of the Hangay Dome (Ionov *et al.* 1998). They also suggest intrusion of asthenospheric material within the lithosphere below 70 km depth. Finally, xenoliths of the uppermost mantle evidence a thermal anomaly that can be related to underplated material (Ionov *et al.* 1998; Ionov 2002).

## 2.3 Structure of the lithosphere from previous geophysical works

Tomographic studies at a global scale have been the main source of constraints on the deep structure of Mongolia until now (e.g. Kulakov *et al.* 1995; Petit *et al.* 1998; Villasenör *et al.* 2001; Friederich 2003; Yanovskaya & Kozhevnikov 2003; Priestley *et al.* 2006; Zhao *et al.* 2006; Kulakov 2008). They generally show with varying degrees of accuracy and consistency, a low-velocity zone located around 100 km depth beneath the Baikal Rift Zone and the Hangay Dome. However, the lateral and depth extensions of this anomaly are not very well resolved and are controversial when compared between different studies (see e.g. a discussion in Zhao *et al.* 2006). Tiberi *et al.* (2003) proceed to a joint inversion of gravity data and traveltimes residuals in the Baikal Rift Zone and demonstrate that a low-velocity anomaly, centred beneath the Baikal Rift, may exist below  $\sim 80$  km depth. However, the lateral extension of the network was not suitable to evidence any connection towards the south and the Hangay deep structure. The gravity signal has also been studied in the same area (e.g. Petit *et al.* 2002; Petit & Déverchère 2006). Three distinct sources for the gravity signal have been proposed: a short-wavelength source arising from lithospheric flexure due to the compressive state, localized on the Sayan and Bogd faults; a hot asthenospheric anomaly located beneath 100 km depth and an anomalous uppermost mantle leading to a local topographic uplift at the apex of the Hangay Dome. However, these studies are based on wavelength separation to localize the anomaly at depth and thus do not solve the non-uniqueness problem of the depth location of the sources.

## 3 DATA ACQUISITION

### 3.1 The MOBAL experiment

In 2001, an international collaborative work between French (CNRS), Mongolian (Mongolian Academia of Sciences) and Russian (Siberian Branch of Russian Academy of Sciences) institutions started for 3 yr. This collaboration was based on an integrated geophysical and geological study and aimed at better understanding the overall geodynamics and lithospheric structure of Mongolia and Baikal regions. Numerous geophysical tools were used: geodesy (GPS), seismology, palaeomagnetism, palaeoseismology and fission tracks (e.g. Calais *et al.* 2003; Calais *et al.* 2006; Mordvinova *et al.* 2007; Vassallo *et al.* 2007; Vergnolle *et al.* 2007; Barruol *et al.* 2008; Petit *et al.* 2008).

The MOBAL seismic experiment was part of this study and aimed to image the lithospheric structures beneath Mongolia and Siberia. A temporary network of 18 broad-band seismic stations were deployed and recorded for 6 months from 2003 April to October. The stations were French TITAN stations with broad-band sensors (CMG40, CMG3 and STS2). They were organized in a roughly N-S profile, starting at the Siberian platform and ending more than 1000 km south near the Gobi-Altai range (Fig. 1). The transect crosses the eastern limb of the Hangay Dome, where abnormal lithosphere or upwelling asthenosphere is suspected.

In this study, we use the teleseismic data recorded by this network to image the crustal and upper mantle. We consider teleseismic events arriving with a first  $P$ -wave signature with an epicentral distance ranging between  $30^\circ$  and  $90^\circ$  (Fig. 2). To pick the first arrival, we filter the signal between 0.1 and 3 Hz. Ultimately, 82 events were selected which produce 1056 traveltimes residuals. The traveltimes residuals are obtained by subtracting the theoretical arrival time, calculated for a standard earth model (IASP91 model, Kennett & Engdahl 1991), from the observed  $P$ -wave arrival time. To get rid of common errors due to bad locations and original time estimation, as well as the deep mantle long-wavelength anomaly, the mean of the

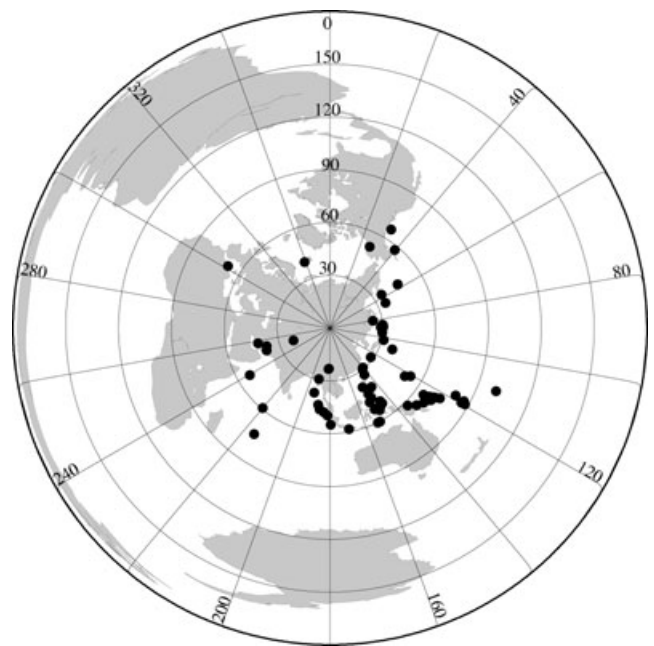


**Figure 2.** Azimuthal distribution of the first  $P$ -wave teleseismic events used for this study (black circles). The projection is centred on the MOBAL network.

traveltime residuals of all stations for a given event was removed from the traveltime residual at each station. We work then on relative traveltime residuals (e.g. Evans & Achauer 1993 for a review). Those residuals range between  $-0.75$  and  $+0.31$  s (Fig. 3) with the largest positive values for stations in the Hangay zone (TUSG and OVGO) and the highest negative values for stations lying on the cratonic shield (KAIT and OKTB). The overall traveltime residuals obtained for the MOBAL experiment are much more positive than the residuals previously obtained for the Baikal transect experiment (Gao *et al.* 1994). We will discuss this observation later.

Despite the heterogeneity of the final Azimuthal distribution of data (Fig. 2), all azimuths are sampled with some events from the Atlantic ridge and two from the Indian ridge. However, we expect the E–W lateral resolution to be poor, owing to the ray geometry mainly coming from the Pacific subduction zone. To overcome this

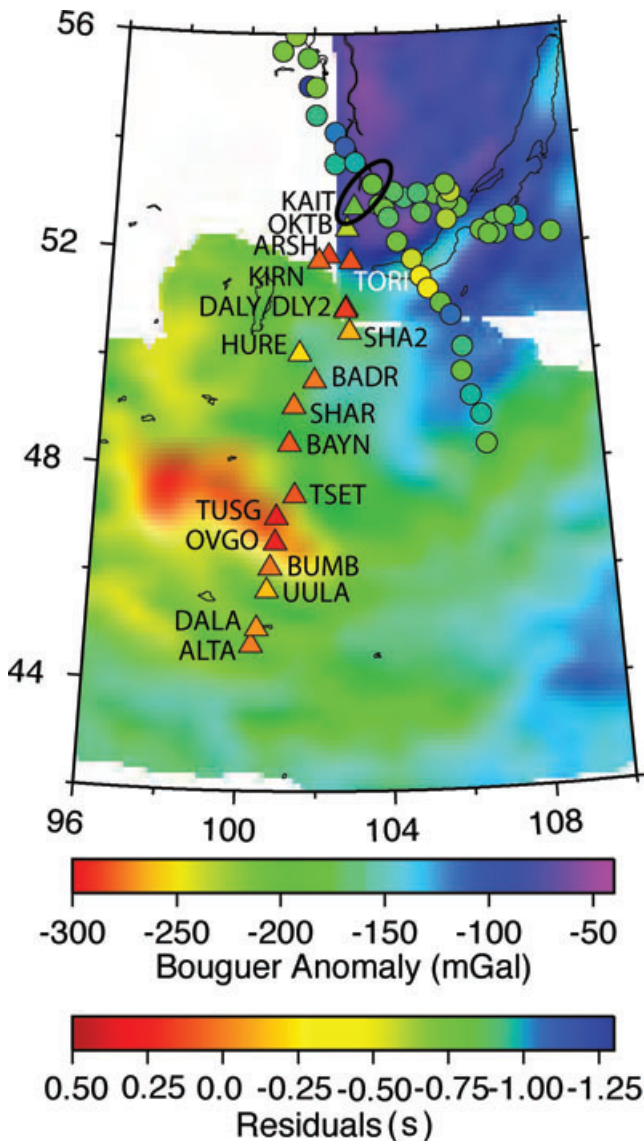


**Figure 3.** Mean relative residuals for the MOBAL experiment stations (triangle) compared with the Baikal Rift experiment (circle, Gao *et al.* 1994). The colour scale of the triangles and circles represents their value in seconds. The Baikal residuals have been referenced according to the KAIT station on the Siberian platform (the two circled stations have the same residuals). Background is the Bouguer anomaly in mGal.

limitation, we consider together the gravity data set, which has a well-resolved spatial distribution in this area.

### 3.2 Gravity data

The second data set we use in this study is the gravity data obtained by merging two databases in Mongolia and Russia (Fig. 3). The first data set is the Bouguer anomaly for the Baikal region, averaged on a  $15' \times 10'$  grid derived from TsNIIGAiK database (Moscow, Russia) by courtesy of G. Demianov. The second data set is an  $8 \times 2.5$  km Bouguer gravity grid, provided by Geophysical Exploration Technology (GETECH, University of Leeds, UK). Bouguer gravity anomalies are terrain-corrected using a mean crustal density of  $2.670 \text{ g cm}^{-3}$  and elevation data from the GTOPO30 database. As we are interested in lithospheric anomalies, and considering the resolution of our models, we filter the data by bandpassing wavelengths between 80 and 120 km. We therefore limit the effect of short wavelength coming from surficial density variations. The resulting signal is very contrasted (Fig. 3) with a large negative long-wavelength ( $-300$  mGal) anomaly corresponding to the Hangay region in the southern part of the MOBAL network and a strong relatively positive signal (up to  $-50$  mGal) near the Siberian Craton. The Altai ranges are underlined by an E–W elongated minimum of  $-225$  mGal.

Assuming a linear positive relationship between velocity and density in the sense of Birch (1961), whenever the sources are common, there should be a negative correlation between residual traveltimes and Bouguer anomaly (Abers 1994). Fig. 4 represents the average residual traveltimes for each MOBAL station against the Bouguer anomaly at the corresponding station location. A negative slope fits all the plots rather well even if some dispersion is observed (correlation coefficient is more than 0.7). We can then reasonably assume that the two signals (gravity and residual traveltimes) have common sources in the study region.

We then perform a joint inversion of these gravity and teleseismic data to quantitatively and efficiently take advantage of both data sets and locate the common sources or perturbations within the lithosphere.

## 4 METHOD

### 4.1 Joint inversion

The method we used was first initiated by Zeyen & Achauer (1997) and then developed by Jordan & Achauer (1999) and Tiberi *et al.*

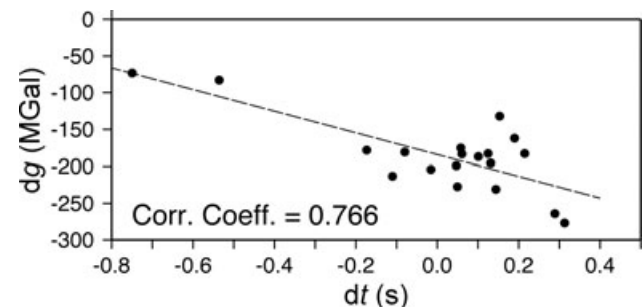


**Figure 4.** Complete Bouguer anomaly ( $dg$ ) as a function of mean delay times ( $dt$ ) for each of the MOBAL experiment broad-band stations. The dashed line is the least-square fitting curve, with a correlation coefficient of 0.766 and a slope of about  $220 \text{ mGal s}^{-1}$ .

(2003). The concept of joint inversion was first mentioned by Lines *et al.* (1988) and has long been developed for different data sets ever since (e.g. Lees & VanDecar 1991; Julia *et al.* 2000). Joint seismic-gravity inversion methods benefit from true simultaneous consideration of traveltime and gravity data, requiring a linear relationship (or a linear approximation of it) between velocity and density. In our scheme, we use the linear positive relation from Birch (1961):

$$\Delta V_p = B \Delta \rho, \quad (1)$$

where  $B$  is the coefficient linking the velocity perturbations ( $\Delta V_p$ ) to the density variations ( $\Delta \rho$ ). Birch (1961) found  $B$  coefficient ranging between 2.5 and 3.5 km s<sup>-1</sup> g<sup>-1</sup> cm<sup>3</sup>, depending on the rock type.

Therefore, the inversion scheme is performed considering three unknowns: the  $P$ -wave velocity anomaly ( $\Delta V_p/V_p$ ), the density contrast ( $\Delta \rho$ ) and the  $B$  coefficient. Assuming  $B$  factor to vary allows for taking into account its statistical variations due to rock types or pressure dependence, while keeping coupling between density and velocity. As the problem is non-linear, we use an iterative least-square method. The algorithm used for the joint inversion in this study is based on a Bayesian approach in which any *a priori* information can be introduced to reduce the set of possible solutions. The method has been extensively detailed in Zeyen & Achauer (1997) and Tiberi *et al.* (2003). We summarize hereafter the main philosophy and assumptions.

The causative sources of the observed gravity anomaly and delay times are supposed to be distributed in  $N$  horizontal layers of thickness  $H_i$ ,  $i = 1, 2, \dots, N$ , in the upper mantle. Every layer is subdivided into  $Nd$  rectangular blocks to which a density contrast is assigned. The velocity is calculated by interpolation using a gradient method between  $Nv$  numbers of nodes for each layer (Thurber 1983). For a given layer, the number  $Nv$  of nodes and  $Nd$  of blocks are independent, allowing for an optimized parametrization for both the density and velocity model. We chose a large enough model to be free of boundary effects.

The average of density and velocity variations for a given layer is assumed to be zero. It is then important to note that the density and velocity contrasts retrieved by the inversion are then relative to each layer and cannot be directly compared from one depth to another.

To find the best-fitting models, the inversion proceeds iteratively in three steps. First, the gravity field due to all blocks of the model is calculated at each observation point, assuming the density contrast of the previous iteration. This forward calculation is achieved by summing the vertical attraction, due to the collection of rectangular blocks in each layer (e.g. Blakely 1995; Li & Chouteau 1998). The delay times are calculated using a bending method, with a 3-D ray tracing through the nodes of the velocity model of the previous iteration (simplex method, Steck & Prothero 1991). The  $B$  coefficient is then calculated for each layer. Only density blocks constrained by velocity nodes (blocks that contain at least one velocity node) are considered for this calculation. Second, the gravity field and delay times are compared with the observed ones, and the residuals are calculated for each data point and station. Finally, we use these residuals to calculate a new density and velocity distribution within the model boundary by a matrix inversion (Tiberi *et al.* 2003). The program stops either when it reaches the required number of iterations or when the difference between observed and calculated data has reached a given minimum threshold.

To restrict the number of possible models that can explain the data set, the inversion introduces a number of *a priori* information and constraints. First, the initial velocity and density models are

a strong *a priori* assertion because it pre-defines the location of perturbations within layers and blocks or nodes. Second, variable standard deviations for both data and parameters are introduced in covariance matrices to avoid a convergence towards unrealistic solutions. Finally, a smoothing constraint is added to avoid sharp and unwilling changes between adjacent density blocks or velocity nodes (see Zeyen & Achauer 1997 for a detailed study).

We conducted several tests to finally obtain the preferred model we present hereafter. We tested various parameters (smoothing, standard deviation, nodes parametrization, model length and width, etc.). For this study, we choose a model made by  $18 \times 26$  nodes and  $12 \times 20$  blocks, distributed in each of the seven layers from the surface down to 300 km depth. The minimum spacing between two nodes is 25 km in E–W and 50 km in N–S directions, according to station spacing. The minimum density block width is 30 and 45 km in E–W and N–S directions, respectively, in accordance with gravity wavelength. The layer depths are 0, 45, 80, 125, 175, 225 and 275 km. We finally invert 10 797 data for 5431 parameters. We fix the maximum number of iterations to six. We start the inversion process with homogeneous density and velocity layers. The velocity standard deviation is 0.01 for all layers and nodes, while the density standard deviation is depth-dependent (from 0.01 at 0 km to 0.02 at 275 km) but constant for a given layer. This is to distribute density variations through the whole volume instead of concentrating the effects on a crustal range. We set the smoothing constraint to 0.001 for both density and velocity, so that the convergence between iterations is always respected.

We also tested node and layer parametrization by varying their location and value. First, the nodes were shifted by 10 km in the east and west directions and by 25 km in the north and south directions. The final root mean square (rms) variation was meaningless compared with the model without node shifting. Only very small short-wavelength differences appear within the resulting density and velocity patterns, smaller than the node spacing. Second, we shifted the layer depths by 10 or 20 km up and down. This allowed us to choose the layer distribution that most minimizes artefacts, but also to better constrain the depth of the different anomalies. We will discuss the latter point for specific anomalies within the discussion part.

## 4.2 Resolution

The resolution of our final model can be estimated by two methods. The first one is the calculation of the resolution matrix at the end of the inversion process, for both density and velocity parameters. This matrix relates the true model to the estimated one and should be close to the identity to reflecting reality (Menke 1984). Most of our inverted parameters exhibit a resolution diagonal term around 0.4, whereas very few show values of 0.7. However, values of the diagonal terms are strongly dependent on the smoothing constraint input into the inversion. In our case, because of noise in the data and short wavelengths unable to be inverted, the smoothing constraint is strong (0.001), and the resulting resolution diagonal terms are hence relatively small.

Another way to test the linear resolving power of our inversion technique is to analyse the ability of our ray geometry to retrieve a given lithospheric structure. The checkerboard test is often seen as a typical approach to test it, as it allows the determination of the smallest wavelength able to be retrieved for a given ray geometry. We place positive and negative velocity and density anomalies ( $\pm 5$  per cent of velocity corresponding to  $\pm 0.1$  g cm<sup>-3</sup> density anomaly)

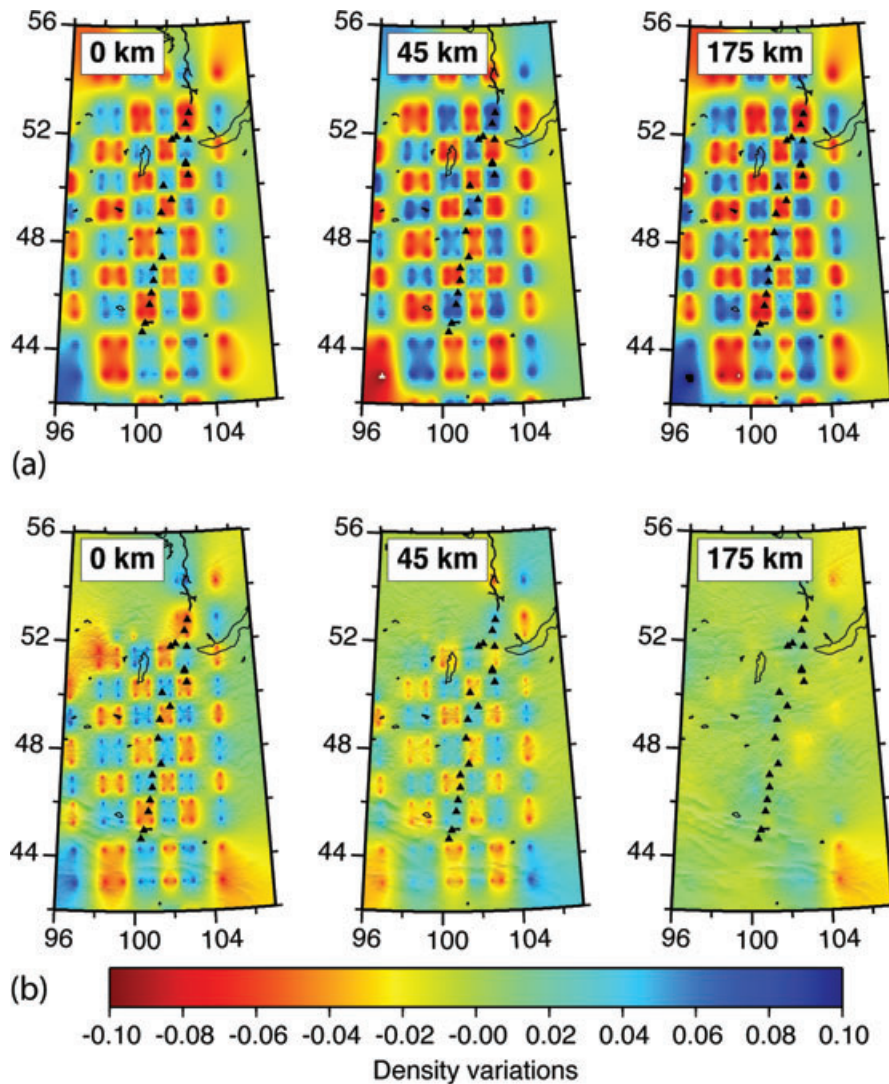


**Figure 5.** Synthetic checkerboard test for density model. (a) Synthetic input density structure. The input density contrast corresponds to an amplitude of  $\pm 0.1$  for a minimum wavelength of 100 km. (b) Recovered density fields for the considered layers over the topography (shaded image).

throughout the 300 km depth of our model (Figs 5a and 6a). The anomaly cell width is  $2 \times 2$  density blocks and at least  $2 \times 2$  velocity nodes. We jointly invert for these synthetic structures using identical model parametrization, as used in the inversion with the actual data distribution. The recovered density and velocity fields are presented in Figs 5(b) and 6(b) for the density and velocity, respectively. The density structures are distinctly retrieved for the two first layers with a total amplitude recovery of 60 per cent. The anomalies initially located at 175 km deep are scarcely imaged in the resulting density inversion (some 20 per cent of retrieval for some positive patches, see Fig. 5b). The degradation of the resolution with depth is due to the gravity signal, quickly decreasing versus the square of the distance. For the velocity, the ray coverage considerably reduces the area of well-determined anomalies (Fig. 6). The first layer is the location of a strong interaction between the shallowest input structures and smearing effects coming from the next layer and is therefore not resolved. The lateral resolution for layers 2 (45 km) to 5 (175 km) is much better, with a clear distinction between fast and slow cells. However, the inversion only retrieves 50 per cent maximum of the input amplitudes (Fig. 6b).

We proceeded to a spike test to evaluate the depth resolution of a single anomaly. We placed a positive velocity and density anomaly of +5 per cent and  $+0.1 \text{ g cm}^{-3}$ , respectively, within the layer 6 (225 km) of our model (Fig. 7). The retrieved model after inversion shows that vertical smearing within the two neighbouring layers (175 and 275 km) is present, resulting in a smaller amplitude for the anomaly. However, we retrieve the initial anomaly in place for both density and velocity (Fig. 7). The lateral resolution is very good, and no horizontal smearing is present.

Although poor density resolution is obvious for depths greater than about 100 km, the lateral and depth resolution is remarkable (Fig. 5b). Vertical smearing is evidenced within the velocity model (Fig. 7b). The weakening of the velocity amplitude is thus directly related to the distribution of signal all along the ray path, and to the lack of non-vertical ray crossing. However, the lateral dimension of the anomalies is correctly retrieved.

The complementary nature of the two data sets is clear from these simple synthetic tests: we expect to have a high-density signal though a poor velocity resolution for the upper crustal part of our model, whereas for the deepest part of our models, the ray crossing

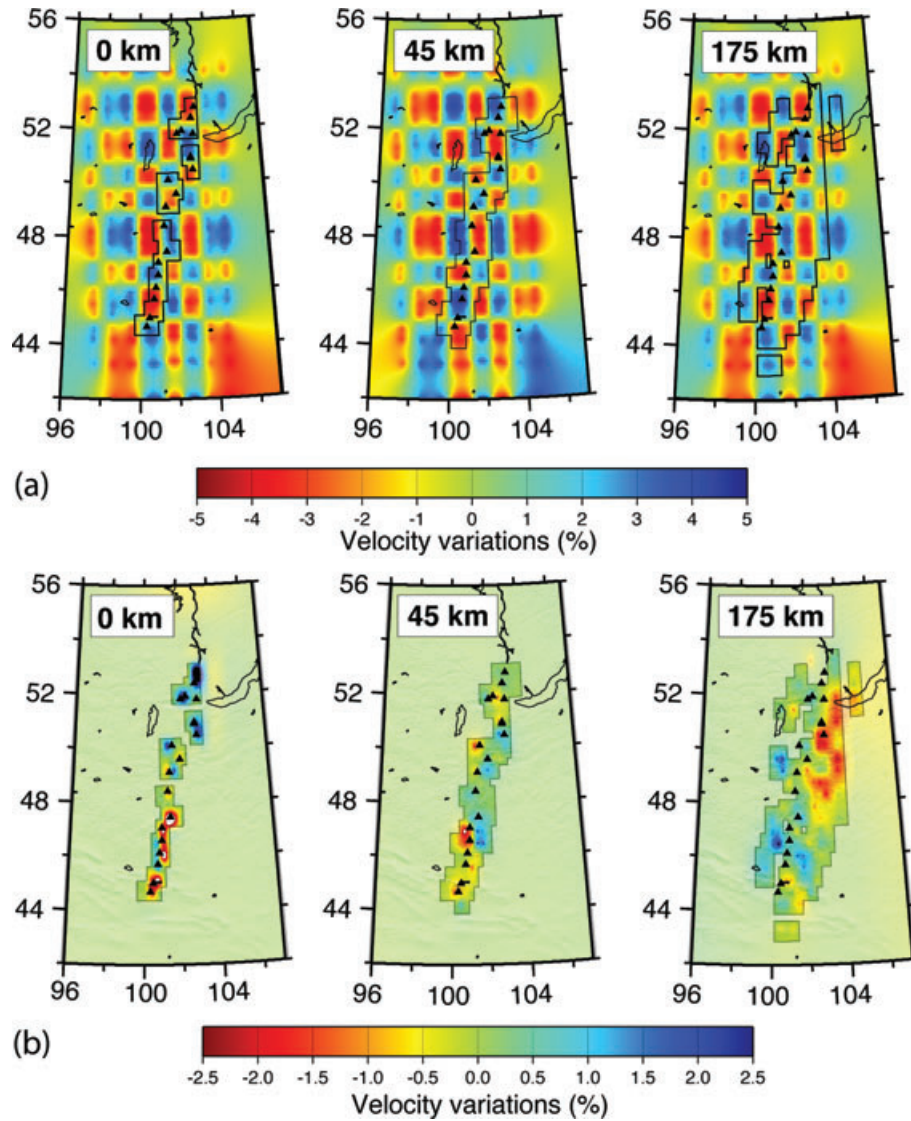


**Figure 6.** Synthetic checkerboard test for velocity model. (a) Synthetic input velocity structure. The input velocity contrast is  $\pm 5$  per cent for a minimum wavelength of 100 km. (b) Recovered velocity fields for the considered layers over the topography (shaded image). The limits of the ray crossing have been reported in (a) to ease the comparison.

will lead to a good velocity image, where the density signal will be the weakest.

## 5 RESULTS

We estimate the stability and robustness of the inversion by checking various criteria. First, the good convergence of the inversion is estimated from the decrease of the rms. In our case, the rms decreases of more than 94 per cent for the gravity and about 43 per cent for the delay times. Besides, the reduction of the total residual sum in our case is 73.9 per cent (data, parameter and smoothing constraint), which is satisfactory. The final density and velocity variations range between  $-0.4$  and  $+0.3 \text{ g cm}^{-3}$  and  $-5$  and  $+5$  per cent, respectively, indicating reasonable values for lithospheric scale.

### 5.1 $B$ factor values

Fig. 8 shows the evolution for  $B$  factor during the inversion. Starting with a uniform value of  $3 \text{ km s}^{-1} \text{ g}^{-1} \text{ cm}^3$ , it ends with values

ranging from 1.2 to  $3.6 \text{ km s}^{-1} \text{ g}^{-1} \text{ cm}^3$ . The smallest  $B$  factors are restricted to layers 2–4 (about 45–100 km depth) and correspond to the poorest correlation between velocity and density (Fig. 8, less than 30 per cent). On the contrary, the highest  $B$  values relate with the highest correlation coefficients (more than 70 per cent). This dichotomy results from the weak velocity resolution for the upper part of the crust. The seismic signal smears along the ray path and acts upon the shallowest layers, leading to a poor correlation with upper density structures. The second effect of vertical smearing is an underestimation of the velocity amplitude for a given layer and hence an underestimation of the  $B$  factor for the same layer. It is then rather difficult to separate true Earth structure effects from artefacts on the resulting  $B$  values.

Due to the ray covering, the resolved part of the lithosphere is concentrated along the profile, with a rather weak lateral extension. Because seismic events mainly come from the east, we only poorly image the western part of Mongolia. We rely on gravity to give us insights into the lateral extension of the mantle structures (Figs 9 and 10).

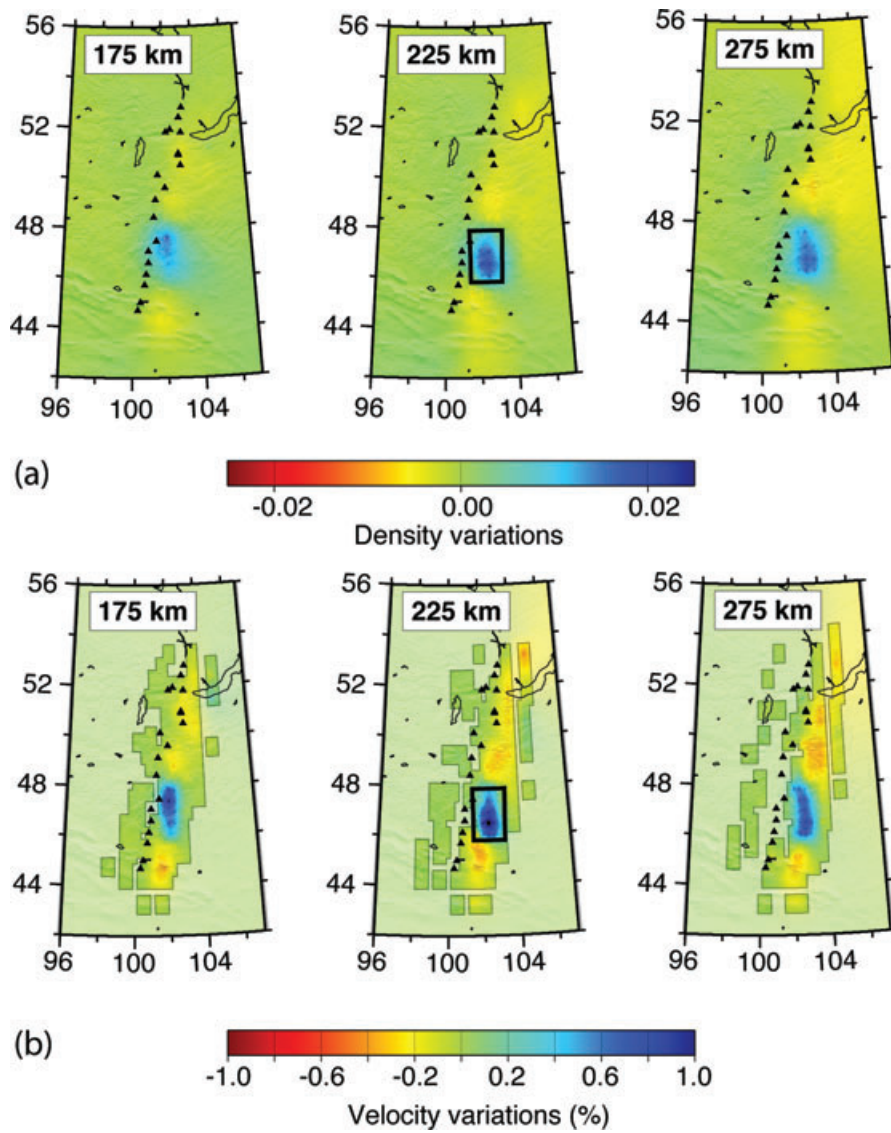


**Figure 7.** Pike synthetic test for (a) density and (b) velocity. The location of the initial perturbation (+5 per cent anomaly at 225 km depth) is indicated by the black rectangle. The resulting models in density and velocity are shown for immediate up and down layers to evaluate the vertical smearing effect in the inversion.

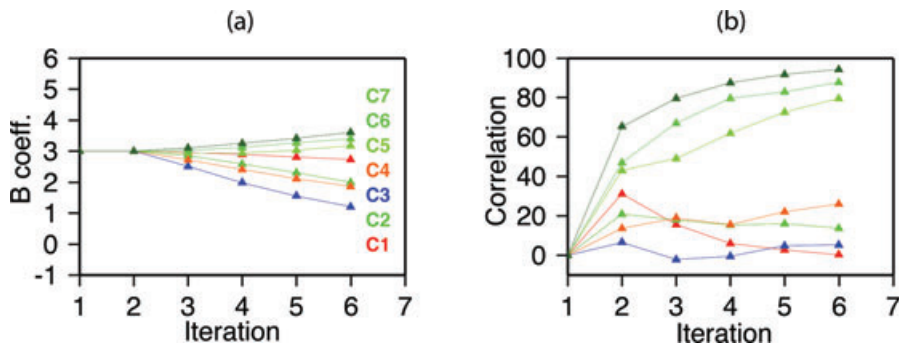


**Figure 8.** (a) Evolution of the  $B$  factor in the Birch-law during the six iterations of the inversion. The indices  $c_n$  refers to the layer number,  $c_1$  being the uppermost one. (b) Evolution of the correlation between density and velocity perturbation for each layer [ $c_1$ – $c_7$ , same colour code as (a)].

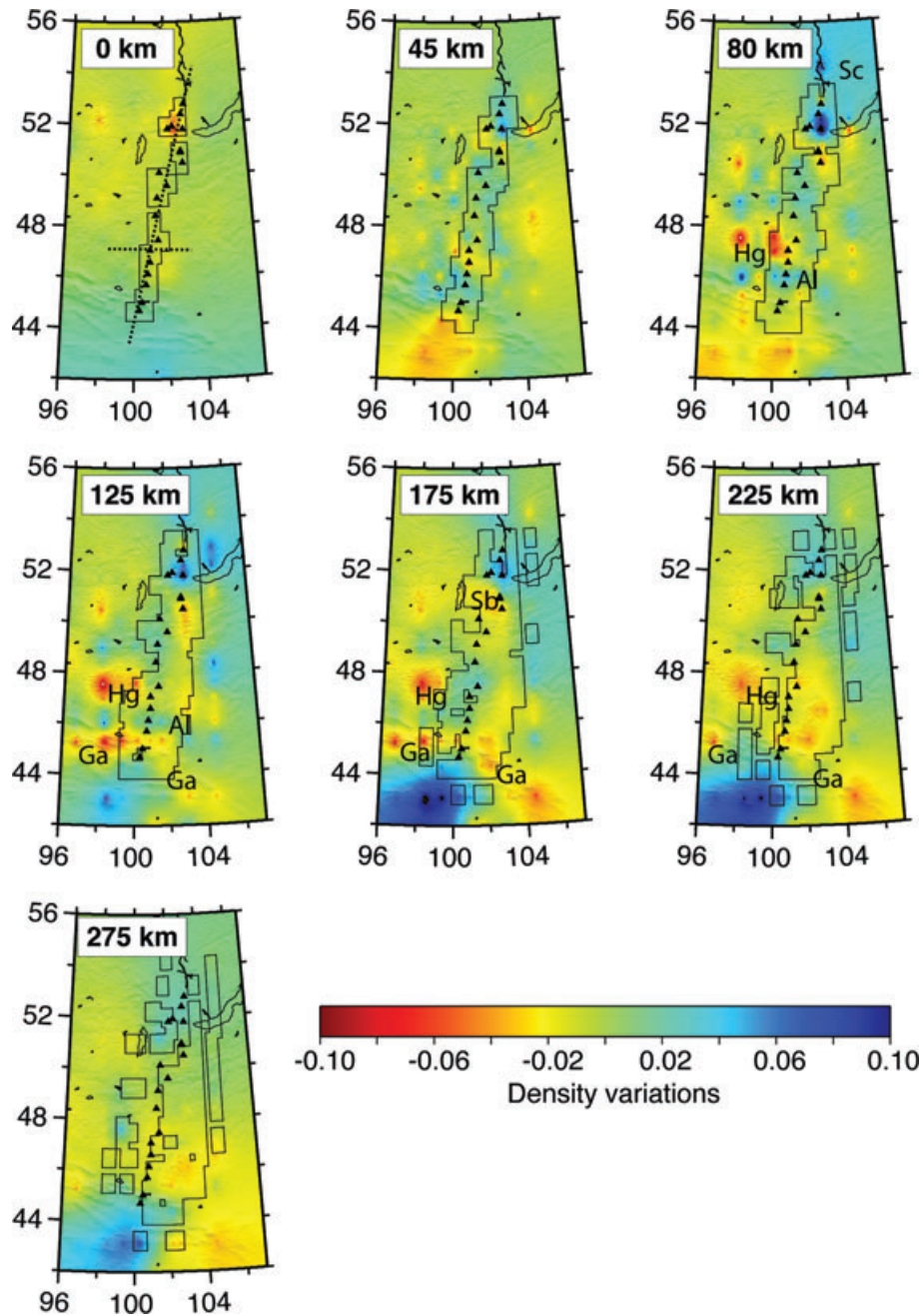


**Figure 9.** Depth slices through the density model after the joint inversion of gravity and teleseismic data. The area where full joint inversion proceeds is delimited by thin black line (density blocks and velocity nodes inverted). Outside this area, only density blocks are inverted. Shaded topography is indicative of main tectonic features. Labels indicate locations of main perturbations discussed within the text: Sc, Siberian Craton; Sb, South Baikal and Sayan belt; Hg, Hangay Dome; Al, Altai; Ga, Gobi-Altai.

## 5.2 Siberian Craton

The cratonic Siberian platform lies on the northernmost part of our study region (Fig. 1). It is well defined in our modelled velocity and density schemes by a high anomaly in both cases (Sc in Figs 9 and 10). The seismic ray paths only reach the southernmost part of the Craton, but the density signal shows that it extends north of our profile. The velocity anomaly is strongly positive and reaches almost +5 per cent, whereas the density contrast we retrieve ranges between +0.06 and +0.1  $\text{g cm}^{-3}$ . We estimate that this anomaly is restricted to the eastern part of the Siberian Craton from its imaging in the density model (Fig. 9,  $z = 80$  km). The depth extent of

this high-velocity/density-body is at least 125 km from the surface (Fig. 11b). From synthetic tests (changing the model layer depth), we can argue that its maximum depth extent is around 150–200 km. The roughly N–S cross-section along the seismic profile shows that the cratonic lithosphere seems to thicken towards the north (Fig. 11b).

## 5.3 Sayan belt

The Sayan belt separates the Siberian platform from the southwesternmost rift basins (Tunka, Hövsgöl and so on, Fig. 1). This fault has only a crustal signature in our models, characterized by a negative

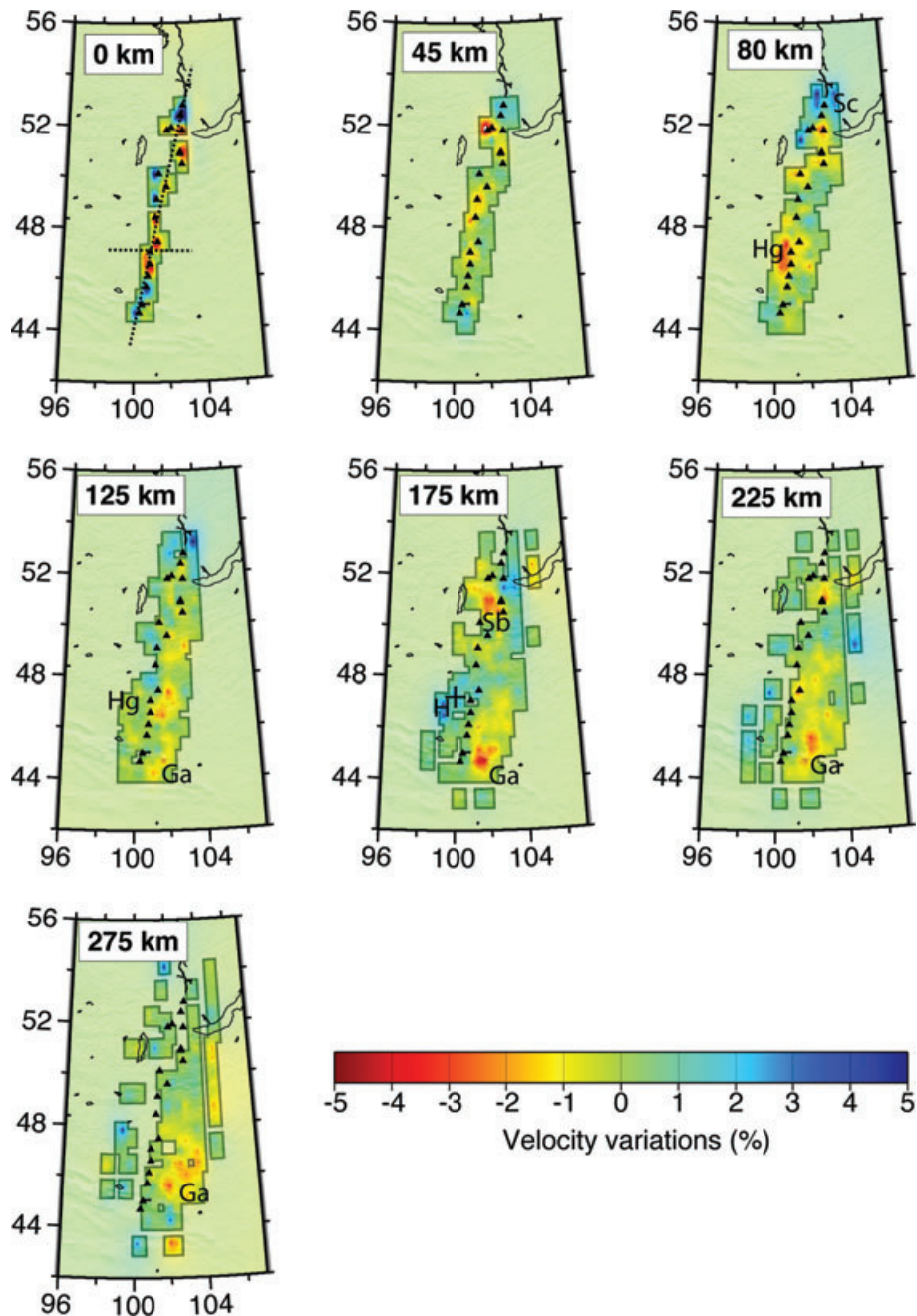


**Figure 10.** Depth slices through the  $P$ -velocity model after the joint inversion of gravity and teleseismic data. The area of nodes really processed during the inversion is indicated as fully transparent. Shaded topography is indicative of main tectonic provinces. Labels indicate locations of main perturbations discussed within the text: Sc, Siberian Craton; Sb, South Baikal and Sayan belt; Hg, Hangay Dome; H+, Hangai positive anomaly; Al, Altai; Ga, Gobi-Altai.

anomaly within the first 45 km near ARSH and KIRN stations, both in velocity and density (Figs 9–11). Since we filtered the gravity signal for the shortest wavelengths, the Sayan belt does not appear obviously on the density layers (Fig. 9). Moreover, the highly dense Siberian Craton is overwhelming the gravity signal at depth, and the low-velocity pattern located at about 100 km depth beneath ARSH station (Fig. 11b) is unseen in gravity.

#### 5.4 South of Baikal Rift Zone

Moving south to the active margin of Siberia, two seismic stations sample this region (DALY and SHA2, Fig. 1). We evidence a

low-velocity and low-density region beneath these two stations for depths ranging between ~60 and ~200 km (Sb in Figs 10 and 11). This anomaly seems to be very restricted laterally as its N–S extension does not exceed 50–100 km. The checkerboard synthetic test shows a very good resolution in this particular area (Figs 5 and 6), and the velocity and density results are very consistent. Moreover, the receiver function analysis from Mordvinova *et al.* (2007) shows two separated low-velocity zones beneath SHA2 stations, one between 80 and 140 km and a deeper one near 200 km, consistent with our models.

It is unclear whether this deep body is actually connected with the crustal negative perturbation beneath Sayan (sites ARSH, TORI).

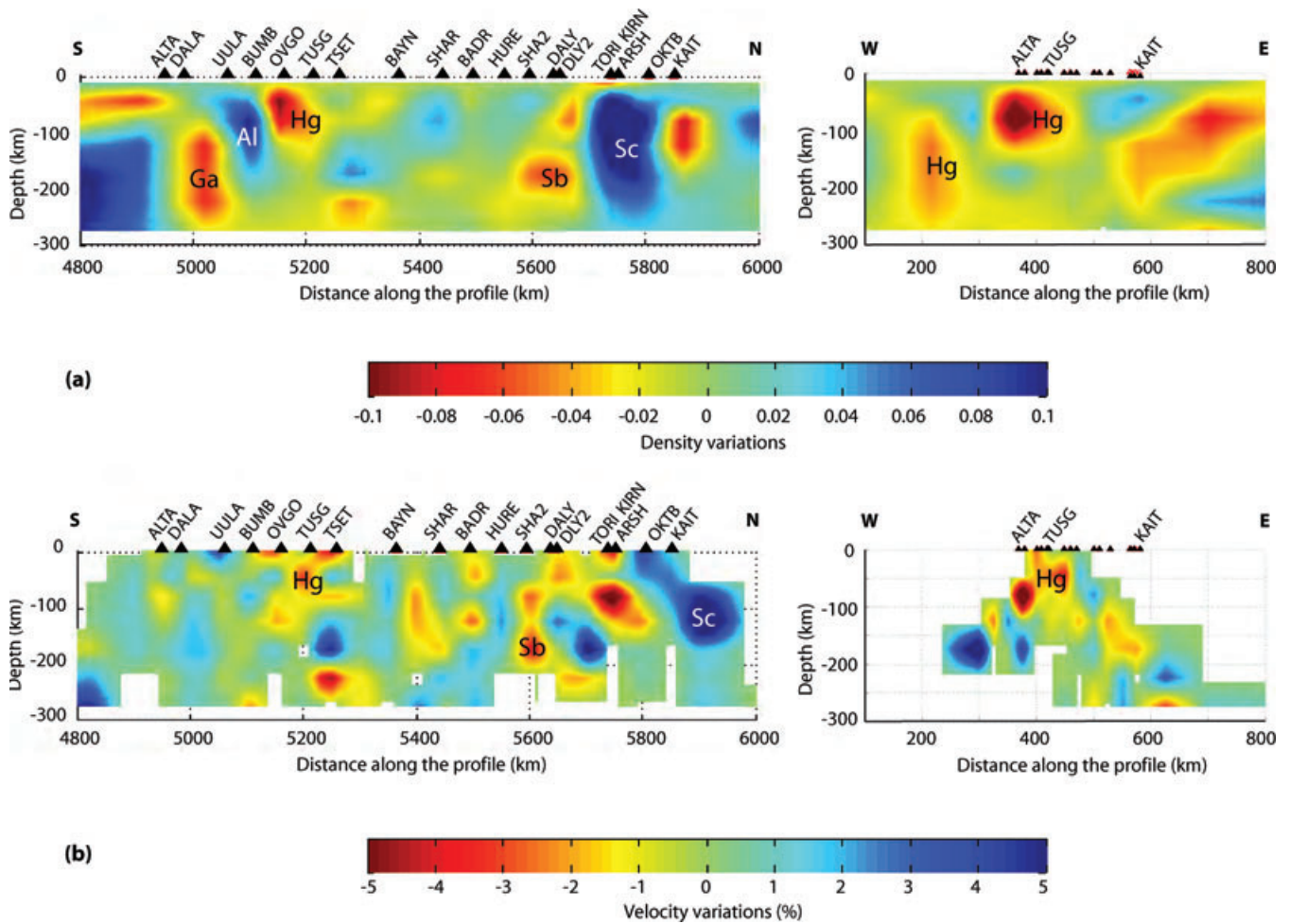


**Figure 11.** Cross-sections for (a) density variations and (b) velocity perturbations along a N–S profile running along the seismic transect (left-hand side) and along an E–W profile at the latitude of station TUSG (right-hand side). The distances are in km related to a UTM projection centred on longitude 102°E. Labels indicate locations of main perturbations discussed within the text: Sc, Siberian Craton; Sb, South Baikal and Sayan belt; Hg, Hangay Dome; Al, Altai; Ga, Gobi-Altai.

They seem connected in the density model (Fig. 11a), but not in the velocity model. The resolution tests (Figs 5 and 6) point out a better resolution for the density than for the velocity in this area and for that depth.

**5.5 Hangay Dome**

The highest topographic feature in the study area is also related to major velocity and density contrasts in our models (sites TSET, TUSG, OVGO, BUMB, Figs 1 and 11). The seismic profile crosses through the eastern end of the Hangay Dome and shows a low-velocity anomaly at this location in the first layer. Then a second negative pattern appears for layers 3 and 4 only (between ~80 and ~125 km, Hg in Fig. 11b). We proceed to different inversions considering various layer depths to constrain the location of the latter anomaly. We finally detect it for depths ranging between 60 and 110 km only. However, when studying the density model, it is clear that west of the profile, where ray crossing is very poor, this anomaly appears deeper (Hg, Fig. 9). The low-density anomaly located beneath the Hangay Dome is thus dipping westwards to reach depths up to 225 km. This is consistent with the gravity study made by Petit *et al.* (2002) for this region, which proposed

a large anomalous body located between 100 and 200 km depth beneath the Hangay Dome. In the present study, we contribute to detail the shape of this anomaly. Rather than a depth constant body, we evidence a westward dipping body. The N–S extension of it seems to be restricted to the Hangay topographic high (Figs 10 and 11a).

**5.6 Altai Mountains**

The easternmost Altai Mountains are located south of the Hangay Dome and are sharply disconnected from it both in velocity and density models. The velocity pattern associated with this belt is not very well resolved, and even if the cross-section of Fig. 11(b) displays velocity contrasts, the ray coverage is quite poor (see checkerboard test Fig. 6), and we prefer not to consider the velocity model as accurate enough there. The density results are far more interesting for they show a very strong contrast north of the Altai Mountains. This belt is separated from the Hangay structure by a very bright dense anomaly of about +0.04 g cm<sup>-3</sup> (noted Al in Fig. 9, sites UULA and BUMB), located from 50 to 150 km depth. This anomaly dips steeply north (Al in Fig. 11a) and isolates the low-density signature of the Hangay Dome from another low but deeper density structure

located south, beneath the highest topography of the Gobi-Altai belt (noted Ga).

This southernmost low-density area is distributed along the whole Altai belt from ~100 km down to ~225 km. It is laterally connected to a low-velocity pattern (*ca.* -4 per cent) from 125 km down to 275 km (Ga in Fig. 10) located east of the network. The western continuity of it in the velocity layer is not straightforward as there is no ray coverage west of the profile, as previously mentioned. Bushenkova *et al.* (2002) also imaged this kind of low-velocity pattern travelling east for depth greater than 130 km. The limited E-W extension of our study cannot help in proving or disproving the lateral extent and dimension of this anomaly. However, it seems of rather high negative amplitude and may be connected with the uppermost part of the Hangay anomaly.

## 6 DISCUSSION

Numerous seismological studies and, more specifically, tomographic analyses have been performed within the study region. We try here to discuss our results in the light of those previous works.

### 6.1 Edge of the Siberian platform

The high-velocity signature of the Siberian Craton is obvious in all tomographic studies of this region. Again, we retrieve the contrast reported between the upper mantle beneath the active orogenic belts and that of the cold, fast Siberian shield. According to Bushenkova *et al.* (2002), there is a high-velocity signature of the Craton down to ~400 km depth, in rough agreement with estimates by Artemieva & Mooney (2001) from heat flow modelling, whereas our models indicate a positive pattern down to only 200 km. This apparent discrepancy can be at least partly solved when considering the spatial sampling and resolution of the tomographic studies. Our sampling of the Siberian Craton is indeed very restricted to its southern part, whereas Bushenkova *et al.* (2002) cover a greater extent of the region. In their model, the southern edge of the Siberian Craton is of negative amplitude after 230 km, and their resolution is weak in this area. The studies can therefore only be tentatively compared.

Our results are in agreement with the thicknesses found from a regional velocity-density model across the southern Baikal Rift (Tiberi *et al.* 2003) and from shear velocity structure (Priestley & Debayle 2003; Lebedev *et al.* 2006). The northward thickening of the Siberian cratonic lithosphere is also consistent with previous works by Zorin *et al.* (1990) and Yanovskaya & Kozhevnikov (2003), which show a thinning of the lithosphere towards the south and the east. Their associated *S*-wave high-velocity anomaly is also constrained to the 150 first kilometres.

### 6.2 Crustal transition from the Craton to the Sayan-Mongolian belt

Our crustal results near the Sayan and Tunka faults are consistent with the recent study by Yakovlev *et al.* (2007). They evidence a low-velocity zone (*ca.* -7 per cent) near the East Sayan and Trans-Baikal mountains down to 43 km depth. Our models (both in velocity and density) show negative anomalies in the same region for the 45 first kilometres (TORI, KIRN and ARSH stations, Fig. 11). Yakovlev *et al.* (2007) propose melts produced by mantle decompression or faults from active deformation in this region, to be responsible for this anomaly. However, the recent receiver function study by Mordvinova *et al.* (2007) clearly indicates a thicker crust beneath TORI,

KIRN and ARSH stations (~50 km) than beneath the Siberian Craton (OKTB and KAIT stations, ~35 km). This abrupt change in crustal thickness fits perfectly with a low-velocity/density pattern beneath the Sayan-Baikal region in our models, without the presence of melt.

South of this anomaly, we locate a low-velocity/density area between ~60 and ~200 km beneath Kamar-Daban (Sb in Fig. 11) coincident with high heat flow and Cenozoic volcanic fields in the region (Kiselev 1987). We observe no clear connection between this Sb anomaly and the Baikal Rift or with the Hangay Dome further south. It is particularly well defined in the velocity pattern that shows the best resolution behaviour for those particular depths (Fig. 11b). Our results are thus consistent with those from Ionov (2002), who proposed a heterogeneous mantle and thermal perturbation in the lithosphere deduced from xenolith studies, rather than a major asthenospheric intrusion below the Moho, related to the Baikal Rift (Gao *et al.* 1994).

In the Hövsgöl-Tunka region, the seismic ray coverage is very poor, and the density model only shows very weak contrasts ( $\pm 0.02 \text{ g cm}^{-3}$ ). This could be indicative of a stable and uniform lithosphere, at least for the wavelengths we considered here (greater than 80 km). The contact of this stable lithosphere with the highly negative signature of Hangay just south of it may favour the development and propagation of huge intracontinental faults like the Bolnai fault (Fig. 1), which exhibits possible rupture nucleation and propagation as deep as 43 and 70 km, respectively during the two large 1905 events (Schlupp & Cisternas 2007).

### 6.3 Relationships to the Baikal Rift system

Part of our network is sampling the southwestern part of the Baikal Rift area. It is therefore interesting to compare our results with the ones from the Baikal Rift experiment from Gao *et al.* (1994). As the teleseismic tomographic inversion results in a non-referenced velocity variation, we cannot directly compare our velocity models with those from Gao *et al.* (1994) or Tiberi *et al.* (2003). To correctly compare results from both experiments, we use the relative time residuals at each station. We take the Siberian platform as the reference, and equal the residuals of station KAIT and station 02 of 1991 experiment (Table 1 in Gao *et al.* 1994) (Fig. 3). Once set at the same reference (Siberian platform), the time residuals actually show different patterns and amplitudes (Fig. 3). The highest residuals (low velocity) are observed for the MOBAL experiment, whereas the Trans-Baikal network shows only negative amplitudes (high velocity). It is clear from Fig. 3 that the strongest low-velocity signal is associated with Central Mongolia and not with the Baikal Rift. We therefore emphasize here that the most important mantle anomaly in the region is located south of the Baikal Rift and not below the Baikal Rift Zone itself, unlike some previous studies (Zorin *et al.* 1990; Gao *et al.* 1994). Most previous tomographic studies lacked the necessary lateral resolution to discriminate between associated anomalies and failed to accurately compare them.

Furthermore, our study shows evidence for a sharp contrast in density and velocity dipping northward at the contact of the Siberian Craton to the folded belt (Fig. 11). We suggest here that the asthenosphere flows upward from beneath the Craton, towards the rift and the adjacent (thinner) Baikal-Mongolian lithosphere, causing decompression melting and sporadic volcanism. This further strengthens existing propositions for the position and development of the Baikal Rift and its southern limit (e.g. Tiberi *et al.* 2003; Lebedev *et al.* 2006; Petit & Déverchère 2006; Barruol *et al.* 2008).

In these models, the rift location at the boundary of a thick cratonic lithosphere may itself provide a mechanism (either through basal drag or pressure gradient related to the western Pacific subduction) to explain the rise of sublithospheric material in the context of slow rifting.

#### 6.4 Roots of the Hangay Dome

First, our models exhibit a negative anomaly right beneath TSET, TUSG and OVGO stations, restricted to within the first 45 km depth in the Hangay Dome region (Fig. 10). We relate this surficial pattern to a thicker crust, as seen by the receiver function analysis for the same stations (Mordvinova *et al.* 2007). Second, our models evidence low-velocity anomalies beneath the same stations for depths ranging between ~60 and 120 km (Hg in Fig. 10), in full agreement with the *S*-velocity model obtained by Mordvinova *et al.* (2007), and a thin lithosphere thickness (Petit *et al.* 2008). The lack of lateral extension of our network prevents us from imaging the mantle velocity west of the profile (Fig. 10). The density model, however, provides an image of this negative anomaly in this region from about 60 km depth down to 225 km (Hg in Figs 9 and 11a). The depth extent of this low-density body has to be considered with caution, as no constraints come from velocity. However, it is in agreement with the study by Petit *et al.* (2002). This anomalous body is restricted to Hangay topographic highs for the first 120 km, but it seems to extend deeper towards the southeast, down to at least 275 km and possibly further (Ga in Figs 9 and 10). This negative anomaly seems to connect to the eastern boundary of the Altai Mountains below 175 km depth. Although the geometry and depth of the anomalies are not exactly the same, a similar overall pattern exists in previous works (Koulakov 1998; Bushenkova *et al.* 2002; Yanovskaya & Kozhevnikov 2003).

Furthermore, the western part of the Hangay Dome is underlain by a high-velocity anomaly at 175 km depth (H+ west of our profile, Fig. 10), a place which is also positively imaged in both Koulakov (1998)'s and Bushenkova *et al.*'s (2002) analyses. This high velocity is located only on the western side of the profile, where Cenozoic volcanism is sparse compared with the eastern side of the profile. For Yanovskaya & Kozhevnikov (2003), this high-velocity (*S* wave) anomaly appears below 200 km. According to Cunningham (1998), this could be the image of a cold continental keel beneath Hangay, driving mantle flow around it. However, a recent SKS study (Barruol *et al.* 2008) shows no strong evidence for such a cold continental keel beneath Hangay. Moreover, this pattern is at the very edge of our seismic network (Fig. 10) and thus only constrained by a very small amount of rays. We thus consider the low-velocity/density mantle beneath Hangay (Hg on Figs 9 and 10) as a continuous body from about 80 km down to 225 km.

Overall from our results, it seems obvious that high-temperature/low-viscosity mantle is acting below the Hangay Dome. It coincides with elevated heat flow values, Cenozoic basalt magmatism, diffuse extension and high surface topography in the Hangay Dome. These observations have since long been used to advocate the possible presence of a juvenile mantle plume in this region (e.g. Zorin *et al.* 1990; Windley & Allen 1993; Kulakov *et al.* 1995; Cunningham 1998; Koulakov 1998). The depth of the low-velocity/density zone we locate beneath Hangay agrees with the depth estimation of partial melting generation from modelling of trace elements in Mongolian basalts (>70 km, Barry *et al.* 2003). The presence and degree of partial melting could be evidenced in the future using *P*-wave and *S*-wave residuals together whenever the latter will be available (e.g. Mavko 1980; Karato 1993). This

ascending flow seems to find its way deep into the mantle below the Altai Mountains (Bushenkova *et al.* 2002). Our finest resolution both in density and velocity can provide more details about the shape and lateral extension than global tomography, and we believe this body has a more complex shape than first suggested.

We thus propose that the central part of Asia has been thermally perturbed by moderate asthenospheric upwelling(s) since, at least, the onset of rifting in the Baikal area. This is consistent with the presence of a weak mantle deduced from models of postseismic deformation in Mongolia (Vergnolle *et al.* 2003). Following Yin (2000), this thermal weakening of the lithosphere may result from mantle upwelling starting at 40–35 Ma and affecting the whole of eastern Asia, favouring the rise of several smaller, tube-like bodies up to the base of the lithosphere. It could then have helped initiate rift development in Tibet and Asia. Note that weak and relatively hot mantle (and possibly lower crust) is also needed below Mongolia to explain viscoelastic relaxation and stress transfer among continental faults, separated by hundreds of kilometres (Pollitz *et al.* 2003).

## 7 CONCLUSION

From joint inversion of gravity and teleseismic data sets, we investigate the crust and upper mantle beneath Central Mongolia along a N–S profile. Our results show no clear evidence for a huge asthenospheric upwelling beneath the whole of Mongolia, connected in any way with the Baikal Rift Zone. Actually, a large difference in delay time residuals between those regions advocates for two different geodynamical mechanisms in each region.

The Siberian Craton is clearly imaged as a high-velocity/density pattern at the northern end of our profile. Its boundary with the Sayan–Baikal region is dipping north, likely causing decompression melting and sporadic volcanism.

North of our profile, we interpret a crustal low-velocity/density zone beneath Kamar-Daban (south of Baikal Rift Zone) to be the effect of a thicker crust, rather than intense melt processes in this region. We evidence two low-velocity/density zones beneath SHA2 and DALY stations, within the eastern Sayan belt, centred around 100 and 200 km depth, consistent with receiver function analyses (Mordvinova *et al.* 2007) and various tomographic models (Koulakov 1998). An anomalous hot mantle here could be responsible for high heat flow and the Cenozoic volcanic field.

A strongly anomalous mantle is found beneath Central Mongolia, related to the Hangay Dome. Our results evidence first a low-velocity/density body within the crust that we relate to the higher thickness of the crust, beneath the stations TSET, TUSG and OVGO (Mordvinova *et al.* 2007; Petit *et al.* 2008). We identify a second low-velocity/density zone from 80 to 150 km, located just beneath our seismic profile near the Hangay Dome. This zone seems to be connected to a wider one, only characterized by a low-density pattern west of our profile. This low-density zone is thicker and located between ~80 and 225 km deep, consistent with previous gravity models (Petit *et al.* 2002). Whether this low-density zone is the location of partial melting is unclear from our analysis; however, this assumption is consistent with trace element analysis of Mongolian basalts, which indicates partial melting at depths greater than 70 km (Barry *et al.* 2003). It is most likely that this hot buoyant material sustains the crust and creates the topographic high of Hangay (Petit *et al.* 2008). At greater depth (275 km and possibly more), this body seems to root towards the southeast.

As a whole, our results show that Central Asia is thermally perturbed by moderate asthenospheric upwelling(s), as also suggested

by global tomographic models, xenoliths studies, elevated heat flow and relaxation models in the region. At long wavelength, two large, plume-like anomalous bodies are found at ~80 and ~100 km depth below the Hangay Dome and the Tunka province, respectively, rooted down to 200–250 km depth. This explains the high topography of the Hangay Dome and the sparse presence of Cenozoic volcanism. Conversely, recent faulting may be the major expression of the India–Asia collision in this region, as well as N–S striking rift basins that connect and interact with major strike-slip faults, such as the Bolnai and Bogd faults.

## ACKNOWLEDGMENTS

This work has been carried out in the frame of the French PICS (Programme International de Coopération Scientifique) number 1251 called ‘*Déformations actives et structures lithosphériques en domaine intracontinental: étude intégrée du système Mongolie-Baikal*’. It has implied a strong cooperation between CNRS (France), Siberian Branch of the Russian Academy of Sciences and Mongolian Academy of Sciences from 2001 to 2004 in palaeoseismology, neotectonics, GPS geodesy and seismology. We thank all partners of this integrative study, especially E. Calais (Purdue University, USA), J.-F. Ritz (Montpellier, France) and V. San’kov (IEC, Irkutsk, Russia). We thank all the people involved in instrumentation preparation, field work and data processing in France, Siberia and Mongolia. We deeply thank Irkutsk and RCAG teams who have participated to the installation/maintenance of the network and the French seismological national pool SisMob. We deeply thank G. Hutton, M. Korn, U. Achauer, I. Koulakov and an anonymous reviewer for their careful and helpful reviews. Figures are from GMT, seismic analysis from SAC. Contribution N°1091 of the IUEM, European Institute for Marine Studies (Brest, France).

## REFERENCES

- Abers, G., 1994. Three-dimensional inversion of regional P and S arrival times in the East Aleutians and sources of subduction zone gravity highs, *J. geophys. Res.*, **99**, 4395–4412.
- Artemieva, I. & Mooney, W., 2001. Thermal thickness and evolution of Precambrian lithosphere: a global study, *J. geophys. Res.*, **106**, 16 387–16 414.
- Barruol, G., Deschamps, A., Deverchère, J., Mordvinova, V.V., Ulziibat, M., Perrot, J., Artemiev, A.A., Dugarmaa, T. & Bokelmam, G.H.R., 2008. Upper mantle flow beneath and around the Hangay Dome, central Mongolia, *Earth planet. Sci. Lett.*, **274**, 221–233.
- Barry, T.L., Saunders, A.D., Kempton, P.D., Windley, B.F., Pringle, M.S., Dorjnamjaa, D. & Saandar, S., 2003. Petrogenesis of Cenozoic basalts from Mongolia: evidence for the role of asthenospheric versus metasomatised mantle sources, *J. Petrol.*, **44**, 55–91.
- Bayasgalan, A., Jackson, J., Ritz, J.-F. & Carretier, S., 1999. ‘Forebergs’, flower structures, and the development of large intra-continental strike-slip faults: the Gurvan Bogd fault system in Mongolia, *J. Struct. Geol.*, **21**, 1285–1302.
- Birch, F., 1961. The velocity of compressional waves in rocks to 10 kilobars, *J. geophys. Res.*, **66**, 2199–2224.
- Blakely, R.J., 1995. *Potential Theory in Gravity and Magnetic Applications*, 2nd edn, Cambridge University Press, Cambridge.
- Burov, E.B., Lobkovsky, L.I., Cloetingh, S. & Nikishin, A.M., 1993. Continental lithosphere folding in Central Asia (part II): constraints from gravity and topography, *Tectonophysics*, **226**, 73–87.
- Bushenkova, N., Tychkov, S. & Koulakov, I., 2002. Tomography on PP-P waves and its application for investigation of the upper mantle in central Siberia, *Tectonophysics*, **358**, 57–76.
- Calais, E., Vergnolle, M., San’kov, V., Likhnev, A., Miroshnichenko, A., Amarjargal, S. & Déverchère, J., 2003. GPS measurements of crustal deformation in the Baikal-Mongolia area (1994–2002): implications for current kinematics of Asia, *J. geophys. Res.*, **108**, doi:10.1029/2002JB002373.
- Calais, E., Dong, L., Wang, M., Shen, Z. & Vergnolle, M., 2006. Continental deformation in Asia from a combined GPS solution, *Geophys. Res. Lett.*, **33**, doi:10.1029/2006GL028433.
- Caporali, A.A., 2000. Buckling of the lithosphere in western Himalaya: constraints from gravity and topography data, *J. geophys. Res.*, **105**, 3103–3113.
- Cloetingh, S., Burov, E. & Poliakov, A., 1999. Lithospheric folding: primary response to compression? (from central Asia and Paris basin), *Tectonics*, **18**, 1064–1083.
- Cunningham, W., 1998. Lithospheric controls on late Cenozoic construction of the Mongolian Altai, *Tectonics*, **17**, 891–902.
- Cunningham, W., 2001. Cenozoic normal faulting and regional doming in the southern Hangay region, central Mongolia: implication for the origin of the Baikal rift province, *Tectonophysics*, **331**, 389–411.
- Delouis, B., Déverchère, J., Melnikova, V., Radziminovitch, N., Loncke, L., Larroque, C., Ritz, J.F. & San’kov, V., 2002. A reappraisal of the 1950 (Mw 6.9) Mondy earthquake, Siberia, and its relationship to the strain pattern at the south-western end of the Baikal rift zone, *Terra Nova*, **14**(6), 491–500, doi:10.1046/j.1365-3121.2002.00445.x
- England, P. & Molnar, P., 1997. Active deformation of Asia: from kinematics to dynamics, *Science*, **278**, 647–650.
- Evans, J. & Achauer, U., 1993. Teleseismic velocity tomography using the ACH method: theory and application to continental scale, in *Seismic Tomography: Theory and Practice*, pp. 319–360, eds Iyer, H. & Hirahara, K., Chapman and Hall, London.
- Flesch, L.M., Holt, W.E., Haines, A.J. & Shen-Tu, B., 2000. Dynamics of the Pacific-North American plate boundary zone in the western United States, *Science*, **287**, 834–836.
- Friederich, W., 2003. The S-velocity structure of the East Asian mantle from inversion of shear and surface waveforms, *Geophys. J. Int.*, **153**, 88–102.
- Gao, S. et al., 1994. Asymmetric upward of the asthenosphere beneath the Baikal rift zone, Siberia, *J. geophys. Res.*, **99**, 15 319–15 330.
- Ionov, D., 2002. Mantle structure and rifting processes in the Baikal-Mongolia region: geophysical data and evidence from xenoliths in volcanics rocks, *Tectonophysics*, **351**, 41–60.
- Ionov, D., O’Reilly, S. & Griffin, W., 1998. A geotherm and lithospheric section for central Mongolia (Tariat region), in *Mantle Dynamics and Plate Interaction in East Asia*, AGU Geodynamics Series, **Vol. 27**, pp. 127–153, eds Flower, M., Chung, S., Lo, C. & Lee, T., American Geophysical Union.
- Jordan, M. & Achauer, U., 1999. A new method for the 3-D joint inversion of teleseismic delaytimes and Bouguer gravity data with application to the French Massif Central, *EOS, Trans. Am. geophys. Un. (Fall Meet. Suppl.)*, **80**(46), F696.
- Julia, J., Ammon, C., Herrmann, R. & Correig, A., 2000. Joint inversion of receiver function and surface wave dispersion observations, *Geophys. J. Int.*, **143**, 99–112.
- Karato, S., 1993. Importance of anelasticity in the interpretation of seismic tomography, *Geophys. Res. Lett.*, **20**, 1623–1626.
- Kennett, B. & Engdahl, E.R., 1991. Travel times for global earthquake location and phase identification, *Geophys. J. Int.*, **105**, 429–465.
- Khutorskoy, M. & Yarmoluk, V., 1989. Heat flow, structure and evolution of the lithosphere of Mongolia, *Tectonophysics*, **164**, 315–322.
- Kiselev, A., 1987. Volcanism of the Baikal rift zone, *Tectonophysics*, **143**, 235–244.
- Koulakov, I., 1998. Three-dimensional seismic structure of the upper mantle beneath the central part of the Eurasian continent, *Geophys. J. Int.*, **133**, 467–489, doi:10.1046/j.1365-246X.1998.00480.x
- Kulakov, I., 2008. Upper mantle structure beneath Southern Siberia and Mongolia, from regional seismic tomography, *Russ. Geol. Geophys.*, **49**, 187–196.
- Kulakov, I., Tychkov, S.A. & Keselman, S.I., 1995. Three-dimensional structure of lateral heterogeneities in P velocities in the upper mantle of the

- southern margin of Siberia and its preliminary geodynamic interpretation, *Tectonophysics*, **241**, 239–257.
- Lebedev, S., Meier, T. & van der Hilst, R., 2006. Asthenospheric flow and origin of volcanism in the Baikal Rift area, *Earth planet. Sci. Lett.*, **249**, 415–424, doi:10.1016/j.epsl.2006.07.007.
- Lees, J.M. & VanDecar, J.C., 1991. Seismic tomography constrained by Bouguer gravity anomalies: applications in Western Washington, *Pure appl. Geophys.*, **135**, 31–52.
- Li, X. & Chouteau, M., 1998. Three-dimensional gravity modelling in all space, *Surv. Geophys.*, **19**, 339–368.
- Lines, L., Schlutz, A. & Treitel, S., 1988. Cooperative inversion of geophysical data, *Geophysics*, **53**, 8–20.
- Logatchev, N. & Zorin, Y., 1987. Evidence and causes of the two-stage development of the Baikal rift, *Tectonophysics*, **143**, 225–234.
- Logatchev, N. & Zorin, Y., 1992. Baikal rift zone: structure and geodynamics, *Tectonophysics*, **208**, 273–286.
- Marotta, A.M., Fernandez, M. & Sabadini, R., 1998. Mantle unrooting in collisional settings, *Tectonophysics*, **296**, 31–46.
- Mavko, G., 1980. Velocity and attenuation in partially molten rocks, *J. geophys. Res.*, **85**, 5173–5189.
- Menke, W., 1984. *Geophysical Data Analysis: Discrete Inverse Theory*, Academic, Orlando, FL, San Diego, CA.
- Molnar, P., England, P. & Martinod, J., 1993. Mantle dynamics, uplift of the Tibetan Plateau and the Indian monsoon, *Rev. Geophys.*, **31**, 357–396.
- Mordvinova, V.V., Deschamps, A., Durgamaa, T., Déverchère, J., Ulziibat, M., Sankov, V.A., Artemiev, A. & Perrot, J., 2007. Velocity structure of the lithosphere on the 2003 Mongolian-Baikal transect from SV waves, *Izvestiya Phys. Sol. Earth*, **43**, 119–129.
- Peltzer, G. & Saucier, F., 1996. Present-day kinematics of Asia derived from geologic fault rates, *J. geophys. Res.*, **101**, 27 943–27 956.
- Petit, C. & Déverchère, J., 2006. Structure and evolution of the Baikal rift: a synthesis, *Geochem. Geophys. Geosyst.*, **7**, Q11016, doi:10.1029/2006GC001265.
- Petit, C., Koulakov, I. & Déverchère, J., 1998. Velocity structure around the Baikal rift zone from teleseismic and local earthquake travel times and geodynamic implications, *Tectonophysics*, **296**, 125–144.
- Petit, C., Déverchère, J., Calais, E., San'kov, V. & Fairhead, D., 2002. Deep structure and mechanical behavior of the lithosphere in the Hangay–Hövsngöl region, Mongolia: new constraints from gravity modelling, *Earth planet. Sci. Lett.*, **197**, 133–149.
- Petit, C., Tiberi, C., Deschamps, A. & Déverchère, J., 2008. Teleseismic traveltimes, topography and lithospheric structure across central Mongolia, *Geophys. Res. Lett.*, **35**, doi:10.1029/2008GL033993.
- Pollitz, F., Vergnolle, M. & Calais, E., 2003. Fault interaction and stress triggering of twentieth century earthquakes in Mongolia, *J. geophys. Res.*, **108**, doi:10.1029/2002JB002375.
- Priestley, K. & Debayle, E., 2003. Seismic evidence for a moderately thick lithosphere beneath the Siberian Platform, *Geophys. Res. Lett.*, **30**(3), doi:10.1029/2002GL015931.
- Priestley, K., Debayle, C., McKenzie, D. & Pilidou, S., 2006. Upper mantle structure of eastern Asia from multimode surface waveform tomography, *J. geophys. Res.*, **111**, B10304, doi:10.1029/2005JB004082.
- Schlupp, A., 1996. Néotectonique de la Mongolie occidentale analysée à partir des données de terrain, sismologiques et satellitaires, *PhD thesis*. Univ. Louis Pasteur, Strasbourg I, pp. 172.
- Schlupp, A. & Cisternas, A., 2007. Source history of the 1905 great Mongolian earthquakes (Tsetserleg, Bolnay), *Geophys. J. Int.*, **169**, 1115–1131.
- Steck, L. & Prothero, W., 1991. A 3-D raytracer for teleseismic body-wave arrival times, *Bull. seism. Soc. Am.*, **81**, 1332–1339.
- Thurber, C., 1983. Earthquake locations and three-dimensional crustal structure in the Coyote Lake Area, central California, *J. geophys. Res.*, **88**, 8226–8236.
- Tiberi, C., Diament, M., Déverchère, J., Petit-Mariani, C., Mikhailov, V., Tikhotsky, S. & Achauer, U., 2003. Deep structure of the Baikal rift zone revealed by joint inversion of gravity and seismology, *J. geophys. Res.*, **108**, doi:10.1029/2002JB001880.
- Vassallo, R., Jolivet, M., Ritz, J.-F., Braucher, R., Larroque, C., Sue, C., Todbileg, M. & Javkhlanbold, D., 2007. Uplift age and rates of the Gurvan Bogd system (Gobi-Altay) by apatite fission track analysis, *Earth planet. Sci. Lett.*, **259**, 333–346, doi:10.1016/j.epsl.2007.04.047.
- Vergnolle, M., Pollitz, F. & Calais, E., 2003. Constraints on the viscosity of the continental crust and mantle from GPS measurements and post-seismic deformation models in western Mongolia, *J. geophys. Res.*, **108**, doi:10.1029/2002JB002374.
- Vergnolle, M., Calais, E. & Dong, L., 2007. Dynamics of continental deformation in Asia, *J. geophys. Res.*, **112**, doi:10.1029/2006JB004807.
- Villasenör, A., Ritzwoller, M., Levshin, A., Barmin, M., Engdahl, E., Spakman, W. & Trampert, J., 2001. Shear velocity structure of central Eurasia from inversion of surface wave velocities, *Phys. Earth planet. Int.*, **123**, 169–184.
- Windley, B. & Allen, M., 1993. Mongolian Plateau: evidence for a late Cenozoic mantle plume under central Asia, *Geology*, **21**, 295–298.
- Yakovlev, A., Koulakov, I. & Tychkov, S., 2007. Moho Depths and three-dimensional velocity structure of the crust and upper mantle beneath the Baikal region, from local tomography, *Russ. Geol. Geophys.*, **48**, 204–220.
- Yanovskaya, T. & Kozhevnikov, V., 2003. 3D S-wave velocity pattern in the upper mantle beneath the continent of Asia from Rayleigh wave data, *Phys. Earth planet. Int.*, **138**, 263–278.
- Yin, A., 2000. Mode of Cenozoic east-west extension in Tibet suggesting a common origin of rifts in Asia during the Indo-Asian collision, *J. geophys. Res.*, **105**, 21 745–21 759.
- Zhao, D., Lei, J., Inoue, T., Yamada, A. & Gao, S.S., 2006. Deep structure and origin of the Baikal rift zone, *Earth planet. Sci. Lett.*, **243**, 681–691.
- Zonenshain, L.P., Kuzmin, M.I. & Natapov, L.M., 1990. *Geology of the USSR: A Plate-tectonic Synthesis*, pp. 242, AGU, Washington, D.C.
- Zeyen, H. & Achauer, U., 1997. Joint inversion of teleseismic delay times and gravity anomaly data for regional structures: theory and synthetic examples, in *Upper Mantle Heterogeneities from Active and Passive Seismology*, pp. 155–168, ed. Fuchs, K., Kluwer Acad., Norwell, Mass.
- Zorin, Y., 1999. Geodynamics of the western part of the Mongolia-Okhotsk collision belt, Tran-Baikal region (Russia) and Mongolia, *Tectonophysics*, **306**, 33–56.
- Zorin, Y., Novoselova, M., Turutanov, E. & Kozhevnikov, V., 1990. Structure of the lithosphere of the Mongolian-Siberian mountainous province, *J. Geodyn.*, **11**, 327–342.